The Astrophysical Journal, 801:5 (8pp), 2015 March 1 doi:10.1088/0004-637X/801/1/5

NEAR-EARTH COSMIC RAY DECREASES ASSOCIATED WITH REMOTE CORONAL MASS EJECTIONS

S. R. Thomas[1,2], M. J. Owens[2], M. Lockwood[2], L. Barnard[2], and C. J. Scott[2]
[1] Mullard Space Science Laboratory, University College London, Holmbury St. Mary, Surrey, RH5 6NT, UK
[2] Department of Meteorology, University of Reading, Reading, RG6 6BB, UK; s.r.thomas@ucl.ac.uk
Received 2014 October 13; accepted 2014 December 25; published 2015 February 23

ABSTRACT

Galactic cosmic ray (GCR) flux is modulated by both particle drift patterns and solar wind structures on a range of timescales. Over solar cycles, GCR flux varies as a function of the total open solar magnetic flux and the latitudinal extent of the heliospheric current sheet. Over hours, drops of a few percent in near-Earth GCR flux (Forbush decreases, FDs) are well known to be associated with the near-Earth passage of solar wind structures resulting from corotating interaction regions (CIRs) and transient coronal mass ejections (CMEs). We report on four FDs seen at ground-based neutron monitors which cannot be immediately associated with significant structures in the local solar wind. Similarly, there are significant near-Earth structures which do not produce any corresponding GCR variation. Three of the FDs are during the *STEREO* era, enabling in situ and remote observations from three well-separated heliospheric locations. Extremely large CMEs passed the *STEREO-A* spacecraft, which was behind the West limb of the Sun, approximately 2–3 days before each near-Earth FD. Solar wind simulations suggest that the CMEs combined with pre-existing CIRs, enhancing the pre-existing barriers to GCR propagation. Thus these observations provide strong evidence for the modulation of GCR flux by remote solar wind structures.

Key words: cosmic rays – Sun: coronal mass ejections (CMEs) – Sun: heliosphere – Sun: magnetic fields

1. INTRODUCTION

When a galactic cosmic ray (GCR) proton enters the atmosphere, it interacts with atmospheric particles and produces a cascade of secondary particles, such as neutrons. Some of these neutrons with high enough energies are able to penetrate through to the surface can be detected by neutron monitors, located at a number of stations at a variety of latitudes and longitudes. Thus neutron count rates serve as an indirect proxy for the top-of-the-atmosphere GCR flux, once the dependence of the atmospheric absorption of neutrons on the atmospheric pressure is considered (e.g., Raubenheimer & Stoker 1974). The standard pressure correction to neutron monitor counts is applied to all neutron monitor stations used in this study.

The flux of GCRs is modulated within the heliosphere on a wide range of timescales. On decadal timescales, GCRs are influenced by differing energetic particle drift patterns and long-term variations in the heliospheric magnetic field (HMF) magnitude and direction (e.g., Jokipii et al. 1977; Thomas et al. 2014a). Over timescales of hours to days, solar wind structures associated with coronal mass ejections (CMEs; Cane 2000) or corotating interaction regions (CIRs; e.g., El Borie et al. 1998; Thomas et al. 2014b) affect GCR flux at Earth. The passage of a CME past an observing spacecraft is frequently associated with an enhancement in the magnetic field magnitude and a variation in the magnetic field direction away from typical Parker spiral orientations (Lepping et al. 1990). If the speed of the CME exceeds that of the surrounding solar wind by greater than the fast magnetosonic wave speed, it will drive a shock front, compressing and heating the ambient solar wind ahead of it in a "sheath" region bounded by the shock and CME leading edge. As GCRs can be scattered by inhomogeneities and discontinuities in the HMF (e.g., Giaclone & Jokipii 1999), the GCR flux at Earth is strongly modulated by the arrival of an Earth-impacting CME, in particular fast CMEs. This can result in GCR flux reducing suddenly over a number of hours, before it recovers to pre-CME levels over a number of days (Forbush 1937; Forbush 1954). Such a temporal variation in GCR flux is commonly referred to as a "Forbush decrease" (FD). Due to the recent "weak" solar cycle (e.g., Lockwood et al. 2012), there have been fewer fast/large CMEs than is normally expected for this phase of the solar cycle (Webb & Howard 2012), and thus we can expect a smaller number of FDs in this period.

A number of studies have investigated how FDs vary with the properties of the driving solar wind structure (e.g., Blanco et al. 2013 and references therein). However, not all FDs are associated with an obvious signature of a CME or CIR seen in near-Earth space. Indeed, Cane et al. (1993) found FDs that appear to have arisen from remote connections with shocks, primarily driven by CMEs propagating from toward the east limb of the Sun. This study provides strong evidence for such modulation of GCRs by remote solar wind structures. In Section 2 we examine a particularly large example of an FD without a significant structure in near-Earth space. In Section 3 we present further events from a period with greater spatial sampling of the heliosphere from the *STEREO* spacecraft. Finally, in Section 4 we use solar wind simulations to provide interpretation of these observations in terms of the global structure of the inner heliosphere.

2. A "PHANTOM" FORBUSH DECREASE

Figure 1 shows a large FD, observed in neutron monitor count rates on the 2002 November 16. The top row shows the percentage change in neutron count rates relative to the 20 day mean for McMurdo (latitude 77.°9 south; longitude 166.°6 east; rigidity cut-off 0.3 GV), Newark (latitude 39.°7 north; longitude 75.°7 west; rigidity cut-off 2.4 GV), Oulu (latitude 65.°1 north; longitude 25.°5 east; rigidity cut-off 0.81 GV), and Alma-Ata (latitude 43.°1 north; longitude 76.°6 east; rigidity cut-off 6.7 GV) in red, blue, green, and orange respectively. The estimated rigidity cut-off values are accessed from the respective neutron monitor's Web site, e.g., the Bartol Institute website for McMurdo and Newark. However, the rigidity cut-off can be influenced substantially by geomagnetic storms and planetary indices such as the Kp index must be considered (Smart et al. 2006).

Figure 1. Forbush decrease on 2002 November 17. The top panel shows neutron monitor counts from McMurdo (red), Newark (blue), Oulu (green), and Alma-Ata (orange). The second panel shows the hourly variability in the near-Earth HMF, δ_B. The near-Earth magnetic field strength, $|\boldsymbol{B}|$, radial solar wind speed, $|\boldsymbol{V}_x|$, and the proton density, n_p, are displayed in the next three panels. The green horizontal line give the 1σ, 2σ, and 3σ occurrences of enhancements of each variable from OMNI2 with respect to the 2001–2003 mean.

During the period shown in Figure 1, each of the neutron monitors show very similar variations, despite the large spread of rigidity cut-offs of the stations. There is a slight spread in the onset timings of the FD due to the longitudes of the stations essentially providing different viewing angles into the heliosphere. Also, it is found from NOAA data that at the time of the FD the Kp index did not increase above a value of 3 ruling out influence on neutron monitor counts from geomagnetic activity.

The second panel shows a measure of the variability in the HMF (δ_B) calculated from the hourly OMNI-2 data set (King & Papitashvili 2005). Here δ_B is the modulus of the differences between consecutive HMF vectors, i.e., $\delta_B = |\boldsymbol{B}_i - \boldsymbol{B}_{i-1}|$. The third panel shows HMF magnitude ($|\boldsymbol{B}|$), the fourth the radial solar wind speed ($|\boldsymbol{V}_x|$), and the final shows the proton density (n_p). In order to objectively assess the presence of potentially GCR-modulating structures in the solar wind, we analyzed the probability distribution functions of all solar wind parameters, using data from 2001 through 2003. From these probability density functions, we calculate the threshold values corresponding to 1σ, 2σ, and 3σ above the mean, which are shown as horizontal green lines in Figures 1–3.

For each station, the neutron count rates reduce from approximately 2%–3% above the background to 4%–5% below it. This represents one of the largest FDs within the neutron monitor data series. Such a decrease in neutron count rates is expected to be due to a sizable GCR barrier in near-Earth space, typically resulting from a large, fast Earth-directed CME or a particularly strong Earth-impacting CIR. Although a CME in near-Earth space identified at this time (Richardson & Cane 2010) primarily on the basis of a reduced proton temperature,

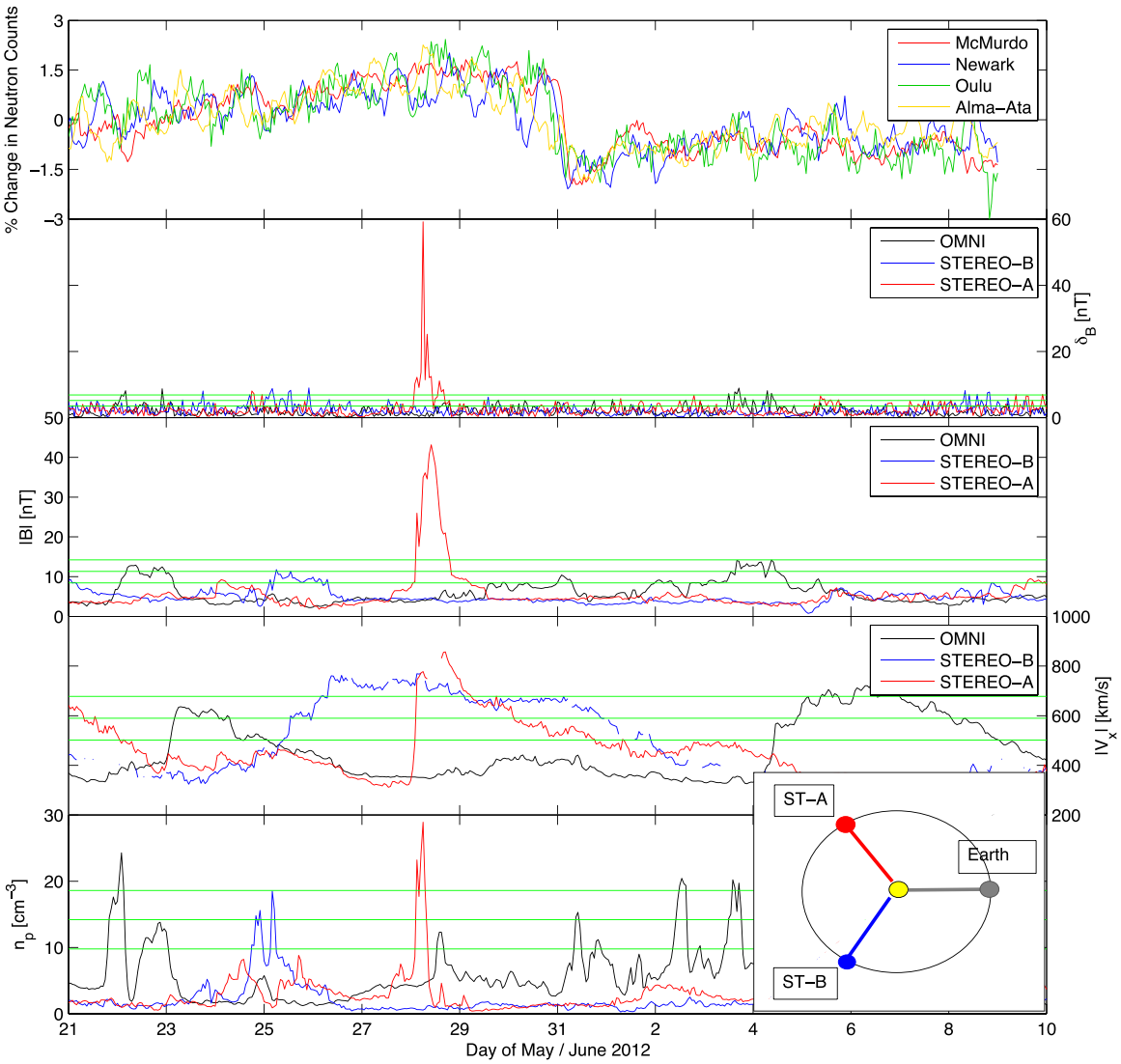

Figure 2. Forbush decrease on 2012 May 30. The top panel shows neutron monitor counts from McMurdo (red), Newark (blue), Oulu (green), and Alma-Ata (orange). The second shows the hourly magnetic field variability, δ_B, in near-Earth space (black), at *STEREO-A* (red) and *STEREO-B* (blue). *STEREO* data are scaled so that the probability density functions match OMNI2 data, to allow direct comparisons of significance. The remaining three panels show (unscaled) magnetic field strength, $|\boldsymbol{B}|$, radial solar wind speed, $|V_x|$ and the proton density, n_p. The green horizontal lines give the 1σ, 2σ, and 3σ from OMNI2 with respect to the 2011–2013 mean. The schematic in the bottom-right gives the approximate locations of the measurement spacecraft.

there is only a small magnetic structure present (an increase of <5 nT, to approximately 10 nT, in hourly data) in the HMF in near-Earth space, which is only in the top 66% of hourly HMF magnitudes observed in the solar wind during this phase of the solar cycle. In addition, there is no significant increase in solar wind velocity or solar wind proton density, but there is a brief and small spike in δB, suggesting that there is some modulating structure in near-Earth space at the time of the FD. However, spikes of this magnitude are common in this 20 day period without associated GCR decreases, thus one might reasonably expect an FD of this magnitude should result from a much greater barrier to the GCRs (e.g., Blanco et al. 2013 and references therein). The most obvious explanation is that the small/weak near-Earth structure is the edge of a much larger CME which was not primarily Earth-directed and thus that the bulk of the GCR modulation was not local. As there is a major FD without an obviously modulating structure in near-Earth space, we refer this kind of event as a "phantom" Forbush decrease (PFD).

In general, the remote modulation effect of a structure of given dimensions will, to some extent, depend on the ratio of event thickness to the GCR gyroradius. For typical GCR energies of a few GeV at a distance of 1 AU from the Sun, the gyroradius would be of the order of 10^5–10^6 km or 10^{-3} to 10^{-4} AU. If the thickness of the modulating structure of a CME is greater than several gyroradii then we expect there to be a significant shielding effect, whereas smaller-scale events will have less of an effect. The expansion of GCR gyroradii with heliocentric distance is closely related to the decrease in HMF strength, as studied by Owens et al. (2008). CMEs evolve in both size and shape as they propagate (Savani et al. 2011). For the 1 GeV GCRs and the extents of the events considered in this study, the dimensions of the CME are much greater than the GCR gyroradii and hence GCR shielding at 1 AU is expected. Indeed, the GCR gyroradius will be further reduced with an increase in the local magnetic field.

Two large solar wind structures in near-Earth space are also seen seven days before (November 9) and three-to-four days

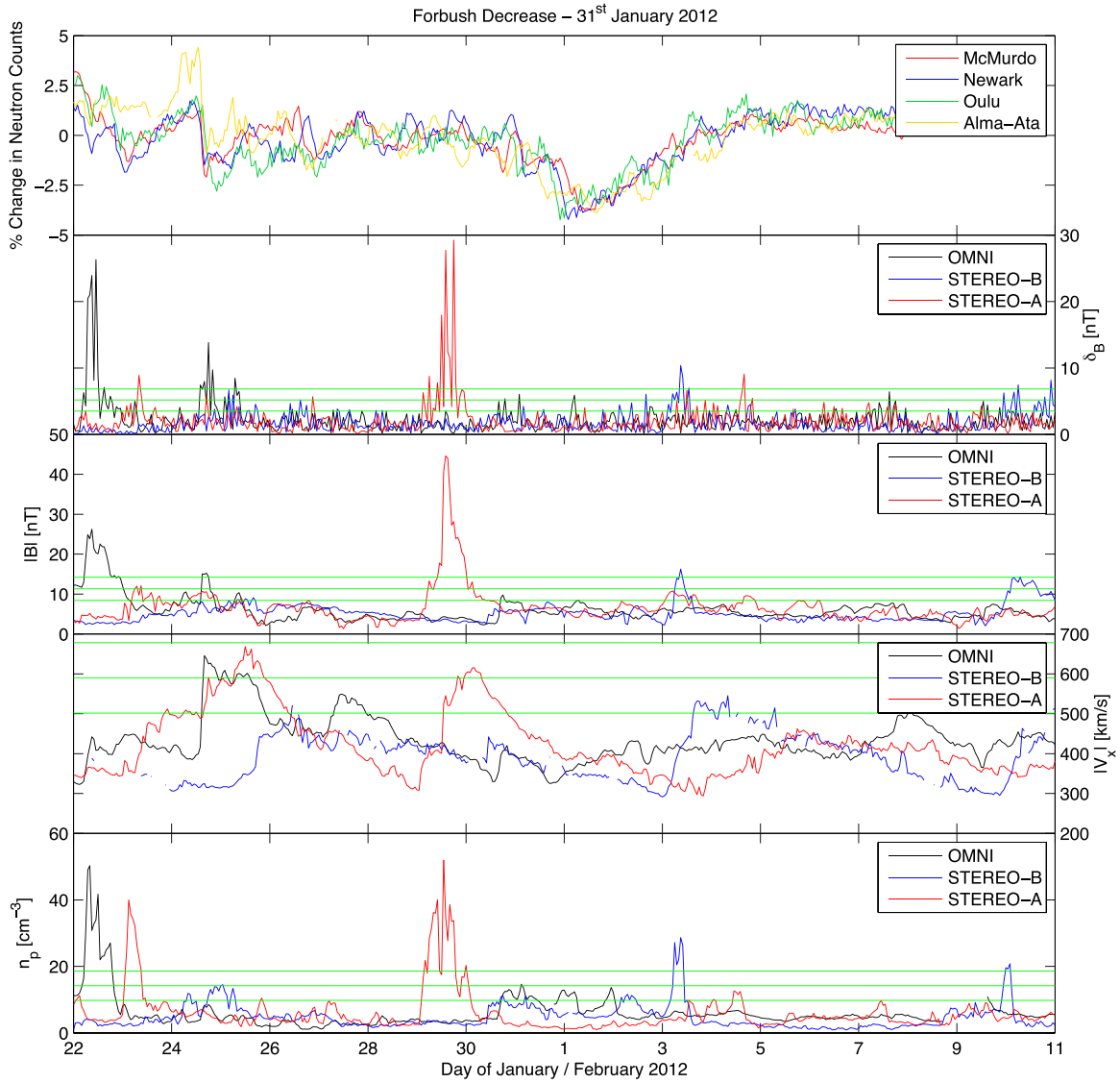

Figure 3. Forbush decrease on 2012 January 31, in the same format as Figure 2.

after (November 20) the large PFD discussed above. Both of these events have significantly larger enhancements in both $|\boldsymbol{B}|$ and δ_B. The November 9 event shows an increase in $|\boldsymbol{B}|$ of approximately 100% over the background level. Within this structure the GCR flux decreases, but this decrease is far more gradual and is not as great in any of the neutron monitors as the PFD on November 16. The November 20 event includes a peak in $|\boldsymbol{B}|$ of approximately 32 nT. This is far greater than the November 9 event but does not coincide with a decrease in GCR flux, possibly as it occurs during the recovery phase from the preceding large PFD. It could, however, also be a highly localized solar wind structure which does not constitute a significant enough GCR barrier to produce a measurable reduction in GCR flux. Clearly, interpretation of GCR modulation requires a more global view of the structure of the heliosphere than can be provided by near-Earth observations alone.

3. "PHANTOM" FORBUSH DECREASES DURING THE *STEREO* ERA

Figure 2 shows an FD beginning on the 2012 May 30, in a similar format to Figure 1. Similar to the 2002 case, the event in Figure 2 shows a significant FD in neutron count rates of approximately 3%–4% at each of the neutron monitors. In this case, the Alma-Ata data, which has the greatest rigidity cut-off, shows a more gradual decrease than the lower rigidity stations. To examine how frequently neutron count rate decreases of this magnitude occur, we apply a running 24 hr mean to the 2011–13 Oulu hourly data and compute the change in neutron count rates over a 24 hr period. Applying this process, the 2012 May 30 FD exhibits a maximum 24 hr decrease of approximately 3% in the Oulu data. Such an FD occurs, on average, less than once a year. Around the time of the FD, the Kp index did not increase above a value of 3 which rules out the influence on neutron monitor counts from geomagnetic activity. Figure 2 shows there is very little structure in the near-Earth solar wind. δB shows no increase outside of the day-to-day variations. Similarly, HMF magnitude, solar wind proton density and radial solar wind speed do not show significant increases at the time of the FD, meaning that any local structure is sufficiently small to rule out GCR modulation solely by local solar wind structures as the primary cause of the FD.

At this time, however, in situ data are also available from the two *STEREO* spacecraft (Kaiser et al. 2008), allowing a total

of three point measurements within the heliosphere at a radial distance of approximately 1 AU. *STEREO-A* was approximately 120° ahead of Earth around the orbit, whereas *STEREO-B* was the same angle behind Earth (see Figure 2 inset schematic). This allows us to include in situ data from *STEREO-A* (red) and *STEREO-B* (blue) for each heliospheric parameter. Solar wind data from 2011–2013 are used to determine the 1σ, 2σ, and 3σ levels discussed previously and shown as green lines in Figure 2. Note that the δ_B estimates for *STEREO* are based on magnetic field components scaled by a factor 0.75, in order to apply the same δ_B thresholds to the *STEREO* and OMNI time series. This only affects the plotted magnitude and not the significance levels of the time series. Figure 2 clearly shows that three days prior to the PFD at Earth, a very large CME is observed at *STEREO-A* which results in magnetic field intensities of nearly 60 nT. Applying a 24 hr running mean to the *STEREO-A* data for 2011–13 reveals that this $|\boldsymbol{B}|$ value occurs in only 0.2% of the data. The CME at *STEREO-A* is driving a shock front, across which the solar wind speed increases from the ambient slow solar speed values of approximately 400–900 km s^{-1} (which exceeds 0.2% of 2011–13 data). The HMF variability, δ_B, rises to a level only exceeded in 0.02% of the 2011–13 hourly data. Clearly, this is a very significant event with enhancement in all heliospheric parameters and particularly intense HMF strength.

Figure 3 shows a second *STEREO*-era PFD beginning late on 2012 January 31, in the same format as Figure 2. This PFD occurs more gradually than the previous two examples, but is still of similar overall amplitude. Applying a 24 hr running mean, it is found that this is a maximum change over a 24 hr period of approximately 4%, which occurs on average every five years in the data. Again the Alma-Ata data shows a more gradual FD than the lower rigidity cut-off stations, but with a similar final magnitude. At the time of the FD the Kp index did not increase above 3, ruling out influence on neutron monitor counts from geomagnetic activity. The near-Earth in-situ solar wind data show a possible small shock front about one day prior to the FD on the 30 January, which appears as a sudden, but small increase in the solar wind speed and proton density. This does not result in a significant |B| enhancement, and only a small increase in δ_B significance levels. More striking is the large CME at *STEREO-A*, which results in an enhancement of $|B| > 40$ nT (greater than 0.2% of data), again 2–3 days before the neutron count rate decline. This occurs at the same time as large spikes of 30 nT in δ_B, 50 cm s^{-3} in n_p, and an increase in the solar wind speed from approximately 300–620 km s^{-1}.

A third PFD during the *STEREO* mission, not shown here for space reasons, occurred on 2012 May 3. The decrease in neutron count rate was in the top 0.1% of the hourly 2011–13 data and again did not coincide with a Kp of greater than 3. This event also involves no significant magnetic or solar wind speed structure in near-Earth space. There is, however, an unexceptional increase in the proton density which could indicate a small transient event. This PFD is again preceded by a large CME at *STEREO-A*, 2–3 days before the FD. In this case the CME at *STEREO-A* is somewhat weaker and less structured than the previous two events, though δ_B is still within the largest 0.5% of the hourly 2011–13 data.

4. HELIOSPHERIC CONTEXT OF EVENTS

As with prior studies of GCR modulation, the 2002 November 16 PFD is difficult to interpret in terms of the global structure of the inner heliosphere, as only a single viewpoint is available for both in-situ observations (from near-Earth spacecraft such as *ACE* and *Wind*) and remote coronagraph observations (from the Large Angle and Spectrometric Coronagraph (LASCO) instrument on *Solar Heliospheric Imager* (*SOHO*)). We therefore focus on the three *STEREO*-era events, which allow three well-separated viewpoints in the heliosphere. For these three PFDs, coronagraphs and Heliospheric Imagers observed extremely fast/wide CMEs erupting close to the west limb of the Sun (viewed from Earth), which are discussed further below. These west-limb CMEs result in the exceptionally large solar wind structures observed at *STEREO-A* 2–3 days prior to the PFDs. Thus, for these three PFDs, the most obvious cause appears to be fast/wide CMEs from the west limb of the Sun, although in general we expect modulation of GCRs by solar wind structures at a range of positions within the heliosphere. Previous studies (Cane et al. 1993) suggest east-limb shocks may be particularly effective at modulating the near-Earth GCR flux, so it is important to also consider possible east-limb structures here. *STEREO-B*, behind the east-limb of the Sun, did not observe any significant CMEs for any of the three PFDs. In the case of the January 31 event, there is also no evidence from coronagraph-based catalogs (such as the LASCO; e.g., Gopalswamy et al. 2009; Robbrecht et al. 2009), the Computer Aided CME Tracking (CACTus) SECCHI-B catalog (Robbrecht & Berghmans 2004), and the Space Weather Database Of Notification, Knowledge, Information (DONKI; accessible from http://kauai.ccmc.gsfc.nasa.gov/DONKI/search/), that a CME passed to the east of Earth, interacting with Earth-connected HMF lines. For the May 30 case, a CME was recorded in the CACTus catalog to the east of the Earth. However, it was not similar to the event discussed by Cane et al. (1993) given that the solar wind speed of 676 km s^{-1} is well within the distribution of "typical" CME speeds.

Thus we proceed with investigating the heliospheric effect of the west-limb CMEs. For this purpose, we used the Community Co-ordinated Modelling Center facility to run the Enlil time-dependent magnetohydrodynamics model with ad-hoc insertion of transient events (Xie et al. 2004). Ambient solar wind conditions were initiated from photospheric magnetograph data using the Wang–Sheeley–Arge model (Arge & Pizzo 2000). To simulate the passage of the CME, a "cone" model of the CME was used to provide the kinematic properties of a transient density plug that was introduced into the magnetogram-derived ambient solar wind simulation. For our application, these input parameters for use in the Enlil model only need to be approximate to give a reasonable physical representation of how the CME could have disturbed the HMF.

Both the 2012 January 31 and the 2012 May 30 events were seen as partial "halo" events by the coronographs on both *STEREO-B* (Cor1) and from the near-Earth LASCO instrument onboard the *SOHO* spacecraft. The times of first observation of the two CMEs by the Cor1 coronagraph on *STEREO-B* were January 27 at 18:54 and May 26 at 21:24, respectively. From Earth, the partial halos were seen to be primarily directed off the Sun's west limb, consistent with interception with *STEREO-A*. Simple geometric arguments about the direction of propagation of the CMEs allows two solutions: either the CMEs had large longitudinal extents, and the partial halos resulted from CMEs propagating away from both *STEREO-B* and Earth, or the CMEs had smaller angular extents but were directed toward either Earth or *STEREO-B* and thus should have been observed in the in-situ solar wind data at either location (to be viewed as a partial halo at either location, some of the CME must be directed either

toward or away from the observer). Given there was no in situ CME observations at Earth or *STEREO-B*, and a clear CME observed at *STEREO-A*, the former explanation better fits the data. Assuming radial propagation, the CMEs must have had large longitudinal extents, as discussed above, with a minimum angular width of 145°. The latitudinal extent of the 2012 January 31 and the May 30 events listed in the CACTus SECCHI-B CME catalog were 176° and 120° respectively. Therefore, assuming a conical model for the CME, we assume a longitudinal extent of the same as the CACTus latitudinal values for these events.

We now focus in particular on the 2012 May 30 event. At this time, *STEREO-A* was at an angle of 115.°8 ahead of Earth in its orbit, while the separation of *STEREO-A* with respect to *STEREO-B* was 127.°0 (see inset of Figure 2 for a graphical representation of this configuration). As the CME propagation direction can only be approximately determined, we assume the partial halo observations from both *STEREO-B* and Earth mean the CME propagates equally away from both vantage points, (i.e., 121.°4 from the Earth–Sun line, ahead of the Earth in its orbit). The CACTus catalog gives the CME major/minor radius of 88.°0 (due to the angular width of 176°) and an initial velocity of 1785 km s^{-1}. These properties are used to characterize the density transient inserted into the Enlil simulation. The CME direction and width values are similar to a previous simulation of this event on the DONKI database.

Figure 4 shows four snapshots of the Enlil model run at 12 UT on 27 (top-left), 28 (top-right) when the CME leading edge was at 1 AU, 29 (lower-left), 30 (lower-right) before the CME passed 2 AU and hence out of the simulation domain. The model results show the solar wind plasma density in the ecliptic plane, where blue colors represent low density and red/white/gray colors represent high densities. On the 27 a weak CIR was approaching Earth. In near-Earth space, this was seen by the slight enhancement in $|\boldsymbol{B}|$ on the 28, prior to the FD, but by comparison with the statistics of CIR effects on GCRs presented by Thomas et al. (2014b), this structure was unlikely to produce an FD in its own right, as it was not associated with a large enough compression of the magnetic field and plasma. The simulation results show that soon after this CIR has passed Earth it interacted with the flank of the CME. Around this time the proton density in the simulated CIR grows via compression, as can be seen from the top-right and lower left panels of Figure 4. The combined CME and the enhanced region of the CIR structure results in a much larger longitudinal extent, which will act as a barrier to GCR propagation. This explanation for the cause of the PFD, however, fails to completely explain the sudden onset of the GCR decrease, as the CME will only enhance plasma densities and magnetic field strength within the CIR locally and the CIR did not modulate GCRs as it passed Earth prior to the PFD.

Enlil simulations of the January and early May CMEs were also performed, though are not shown here. The 2012 January 31 example shows a similar large-scale heliospheric structure to the May/June example in Figure 4, with the CME interacting with a CIR after it has passed Earth. However, the May 3 event does not show CIR interaction in the same way, and the CME also has a smaller longitudinal extent. We note that for this event there is a further CME that erupted to the east of the Earth-Sun line that could have modulated the GCR flux in the manner proposed by Cane et al. (1993). However, if such a CME alone was the cause of the PFD, one would expect PFDs to be far more common than observed, as this CME was not an unusually dense or fast.

5. DISCUSSION AND CONCLUSIONS

This study has presented four large FDs which are not readily associated with significant solar wind structures, such as CMEs or CIRs, in the near-Earth space. In these PFD events the GCR modulation must be primarily the result of heliospheric structures far from Earth. Such remote GCR modulation has previously been suggested (Cane et al. 1993), but has been difficult to verify due to limited spatial sampling of the heliosphere. For three of the four PFDs considered in this study, however, *STEREO* spacecraft allow both in situ and coronagraph observations from three well-separated points in the inner heliosphere. In each case, an exceptionally large CME passed over the *STEREO-A* spacecraft, located behind the west-limb of the Sun, 2–3 days prior to the PFD at Earth. For the events of 2012 May 30 and 2012 January 31, the CME which passed *STEREO-A* also merged with a previously weak CIR which caused no modulation when it previously crossed Earth, to generate a magnetic barrier with a greater longitudinal extent to GCRs than just the remote CME itself. We suggest that this confluence of two heliospheric structures may be the reason for the scarcity of PFDs.

It is important to note that remote structures at other locations in the heliosphere may also result in modulation of GCR flux at Earth, but that either the configuration of *STEREO* spacecraft was particularly sensitive to modulation associated with west-limb CMEs or that west-limb CMEs are most effective at modulation near-Earth GCR flux. It may also be the case that west-limb CMEs provide greater modulation of GCRs at Earth at this particular phase of the solar cycle, given that all PFDs we have described have taken place in the same year, while there have been large, west-limb CMEs at different phases in the cycle. Furthermore, it is also clear that not all wide/fast west-limb CMEs, even around 2012, result in a PFD at Earth. In particular, the extremely fast CME on the 2012 July 23, which had one of the shortest 1 AU transit times ever observed (e.g., Liou et al. 2012), crossed *STEREO-A* without causing a substantial drop in neutron count rates at Earth. This is further reason to postulate that the combined effect of a CIR and a CME is necessary to produce a sudden decrease in GCR flux at Earth, but this remains to be demonstrated.

Further work is required to quantitatively model the response of GCRs in PFDs, as it is by no means obvious why a coupled CIR-CME would cause such a rapid decrease in neutron monitor count rates. We do note that the PFD onset time is around the time that the CME leading edge reaches approximately 4 AU, when it is expected to first encounter Earth-connected magnetic field lines (e.g., assuming a Parker Spiral field and an average radial CME speed of 1000 km s^{-1}, the time taken for the May 26 CME to reach the Earth-connected HMF would be 4.7 ± 1.0 days, depending on the precise HMF configuration and deceleration rate of the CME. This fits well with the observed time from CME launch to FD of approximately 4 days.)

We are currently working on a full statistical study of PFDs and solar wind structures in order to fully establish the heliospheric configurations responsible for remote modulation of near-Earth GCR flux. The use of low latitude muon telescopes will give further information on the modulation of high rigidity particles. A preliminary study of these events show a similar but more gradual FD than the neutron monitor data, but further work is required here. In addition to this, quantitative modeling of GCR transport during such events is required to explain the relatively sudden nature of PFDs.

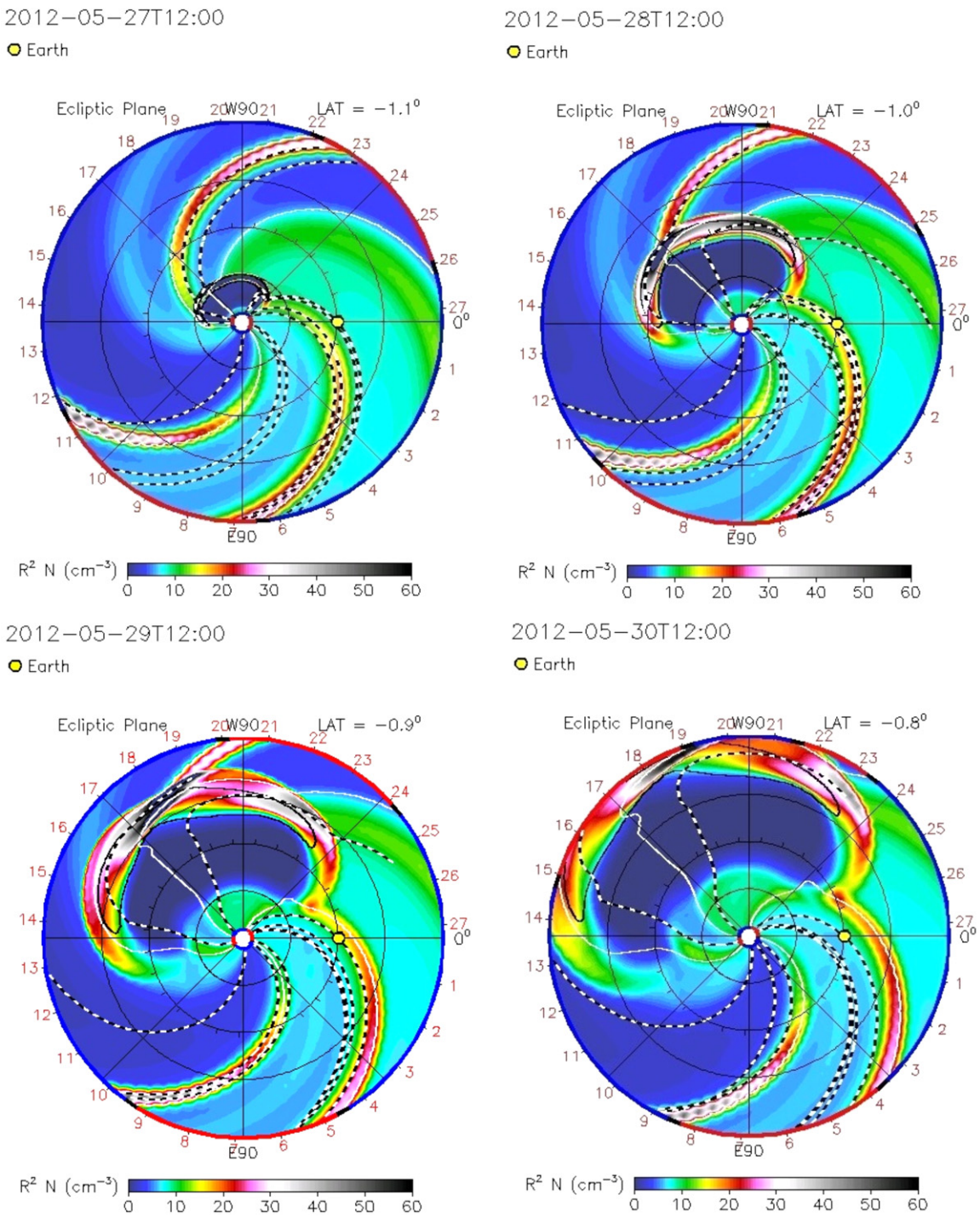

Figure 4. Snapshots of the Enlil model run at four times during the 2012 May 30 CME's propagation through the inner heliosphere. The dates shown are for 12 UT on 27 (top-left), 28 (top-right), 29 (lower-left), and 30 (lower-right). Blue colors represent low proton density and red, white and gray represent very high density. Earth is marked as the yellow circle and the Sun is the white circle.

We are grateful to the Space Physics Data Facility (SPDF) of NASA's Goddard Space Flight Center for combining the data into the OMNI 2 data set which was obtained via the GSFC/SPDF OMNIWeb interface at http://omniweb.gsfc.nasa.gov. We thank the Bartol Research Institute of the University of Delaware for the neutron monitor data from McMurdo and Newark, which is supported by NSF grant ATM-0527878, the University of Oulu for the Oulu neutron monitor data, and the Ionosphere Institute of Kazakhstan Republic for the Alma-Ata neutron monitor data. We thank the Community Co-ordinated Modeling Center for the ENLIL model run. We also acknowledge the use of the *SOHO* LASCO CME catalog which is generated and maintained at the CDAW Data Center by NASA and The Catholic University of America in cooperation with the Naval Research Laboratory, as well as the CACTUS catalog compilers (Royal Observatory of Belgium) and the NASA Goddard's DONKI CME database. S.R.T. is supported by a studentship from the UK's Natural Environment Research Council (NERC).

REFERENCES

Arge, C. N., & Pizzo, V. J. 2000, JGR, 105, 10465
Blanco, J. J., Catalán, E., Hidalgo, M. A., et al. 2013, SoPh, 284, 167
Cane, H. V. 2000, SSRv, 93, 55
Cane, H. V., Richardson, I. G., & von Rosenvinge, T. T. 1993, JGR, 98, 13295
El Borie, M. A., Duldig, M. L., & Humble, J. E. 1998, Pl&SS, 46, 439
Forbush, S. E. 1937, PhR, 51, 1108
Forbush, S. E. 1954, JGR, 59, 525
Giaclone, J., & Jokipii, J. R. 1999, ApJ, 520, 204
Gopalswamy, N., Yashiro, S., Michalek, G., et al. 2009, EM&P, 104, 295
Jokipii, J. R., Levy, E. H., & Hubbard, W. B. 1977, ApJ, 213, 861
Kaiser, M. L., Kucera, T. A., Davila, J. M., et al. 2008, SSRv, 136, 5
King, J. H., & Papitashvili, N. E. 2005, JGR, 110
Lepping, R. P., Burlaga, L. F., & Jones, J. A 1990, JGR, 53, 11957
Liou, K., Wu, C.-C., Dryer, M., et al. 2012, J. Atmosph. Solar-Terrestrial Phys., 121, 32
Lockwood, M., Owens, M. J., Barnard, L., Davis, C. J., & Thomas, S. R. 2012, A&G, 53, 3.09
Owens, M. J., Arge, C. N., Crooker, N. U., Schwadron, N. A., & Horbury, T. S. 2008, JGR, 113, A12103
Raubenheimer, B. C., & Stoker, P. H. 1974, JGR, 79, 5069
Richardson, I. G., & Cane, H. V. 2010, SoPh, 264, 189
Robbrecht, E., & Berghmans, D. 2004, A&A, 425, 1097
Robbrecht, E., Berghmans, D., & van der Linden, R. A. M. 2009, ApJ, 691, 1222
Savani, N. P., Owens, M. J., Rouillard, A. P., et al. 2011, ApJ, 731, 109
Smart, D. F., Shea, M. A., Tylka, A. J., & Boberg, P. R. 2006, AdSpR, 37, 1206
Thomas, S. R., Owens, M. J., & Lockwood, M. 2014a, SoPh, 289, 407
Thomas, S. R., Owens, M. J., Lockwood, M., & Scott, C. J. 2014b, SoPh, 289, 2653
Webb, D. F., & Howard, T. A. 2012, LRSP, 7, 3
Xie, H., Ofman, L., & Lawrence, G. 2004, JGR, 109, A03109